A Multi-layer Perceptron Approach to Automatically Detect Tissue via NIR Multispectral Imaging

Sandeep Gurm, University of Waterloo, ON, Canada
Ossama Badawy, University of Waterloo, ON, Canada
Alexander Wong, University of Waterloo, ON, Canada

Abstract

We present a novel pixel-level spectra based multi-layer perceptron (MLP) to discriminate regions of biomedical multispectral imaging data into two categories: tissue and non-tissue. The spectra used for this study are 740nm, 780nm, 850nm, and 945nm as these wavelengths are on either side of the isosbestic point for oxyhemoglobin and deoxyhemoglobin; absorbers that are common in all healthy tissues. An MLP is trained using multispectral data from 12 human subjects and 12 non-tissue objects. The MLP is tested on three multispectral challenge image sets, from which the accuracy, sensitivity, and specificity of the model yield results of 91.3% (+/-0.2%), 98.1% (+/-0.3%), and 88.5% (+/- 0.3%) respectively.

1 Introduction

Multispectral imaging (MSI) originated in the field of remote sensing and has grown to various areas of application such as; art restoration, food quality, crime scene detection, etc [1].

In the field of medical imaging, near infrared (NIR) multispectral imaging has become a common technique to non-invasively and quantitatively evaluate tissue health [2], especially in disease diagnosis and image guided surgery [1].

The problem that this research paper will address is identifying regions in multispectral images that are either tissue or non-tissue. This is an important first step in tissue characterization as well as image segmentation.

To characterize multispectral images, several approaches have been taken by researchers. A particularly effective approach has been to utilize a multi-layer perceptron (MLP), which has shown excellent potential to classify cancerous tissues in both visible and NIR imaging regimes, as is demonstrated in the research put forward by Jolivot et al [3] and Carrara et al [4]. This work shows excellent promise for using an MLP for the purposes of classifying tissue.

Much of the contemporary research on tissue classification focuses on finding important diagnostic information; the aim of this paper is not to classify specific structures, cancers, or lesions. Rather, this paper will look to build a novel MLP architecture which will generally classify areas of MSI data that are either tissue or non-tissue. The motivation for doing this is to help make MSI applications more efficient; in real-time imaging applications, knowing tissue/non-tissue regions in a MSI imaging field can help reduce computational overhead by only processing relevant sections of the image. To the best of the authors' knowledge, this approach to general tissue classification has not been previously proposed.

2 Methodology

2.1 Light-tissue interaction

To understand the context of this work, it is necessary to first gain a basic understanding of tissue optics.

As NIR light is delivered to biological tissue, absorption and scatter of light occurs due to the structure of the tissue as well as the composition of various components, such as hemoglobin, melanin, and water/fat content [5]. The components of tissue have their own distinct scattering and absorption characteristics. Each component will absorb or scatter differently based on wavelength, and as such, wavelengths of light can be selected to build a mixed mathematical model to solve for these components [5]. The absorption of these components can be generally modeled as:

$$T = e^{-u_a L} \tag{1}$$

Where T represents the transmission of light (as a fraction), u_a is the absorption coefficient of the component of interest, and L is the path length of the material [5].

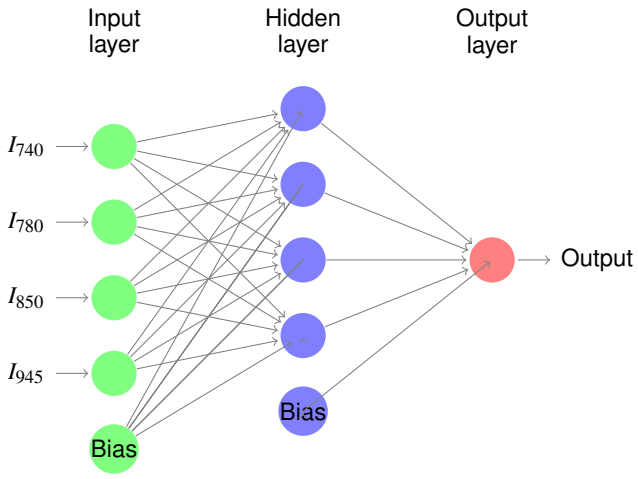

Fig. 1: The architecture of the single layer MLP - I_λ is the input average pixel-level spectra from each wavelength. All connections between layers and nodes signify weights which are solved for by the back-propagation method. Output of the MLP is a decimal value between 0 and 1 (above or equal to 0.5 =tissue, below 0.5 = non-tissue). Each node signifies the sigmoid activation function

The absorption, u_a, is wavelength dependent. As such, to quantitatively determine the amount of the desired component in tissue, multiple wavelength measurements of the transmission (or reflectance) must be calculated to create an accurate model - this is the basis of MSI [6].

For this research, oxyhemoglobin and deoxyhemoglobin are considered, as these components are common across all types of human tissue. Four wavelengths are selected at 740nm, 780nm, 850nm, and 945nm; these wavelengths are selected for their location on the isosbestic point of the oxyhemoglobin/deoxyhemoglobin absorption curves [5].

2.2 Architecture of MLP Model

To classify tissue/non-tissue for MSI data, we propose a design of an MLP which uses pixel-level spectra as inputs and a hidden layer with the same corresponding number of nodes; i.e. given *n* wavelengths, there will be *n* number of nodes which will take the pixel-level spectra of each wavelength as an input (plus a bias node). There is 1 hidden layer which also contains *n* nodes (plus a bias node). The diagram of the specific MLP architecture created for this research is shown in Figure 1, which is for four wavelengths.

I_λ denotes the average pixel-level spectra at each wavelength. All the connecting lines represent a weight that relates the input to the hidden layer, and the output of the hidden layer to the output layer. The activation function used for each node is the sigmoid function. The output of the MLP is a decimal number between 0 and 1, which can be used to estimate the presence of tissue in accordance to the labels given to the data (i.e. tissue=1, non-tissue = 0).

2.3 Training the MLP Model

A clinical MSI data-set was mined from a previous study. Grayscale multispectral images were captured at 4 different wavelengths: 740nm, 780nm, 850nm, and 945nm; the images were captured with a custom built NIR illumination and imaging system. The four images are captured sequentially, within 20ms of one another to ensure minimum disturbance from movement. All images taken were of subject's forearms.

The MLP was trained using data from 12 subjects (tissue) and 12 non-tissue objects that appear in the images. The data set was augmented by accounting for the standard deviation in the data set,

and adding randomly generated data points to the oiriginal data set within the standard deviation.

Pixel-level spectra were manually sampled from each image that had instances of tissue and non tissue across all wavelengths in a 10 pixel by 10 pixel region of interest (ROI) - these pixel-level spectra averages were the inputs to the MLP for building the model.

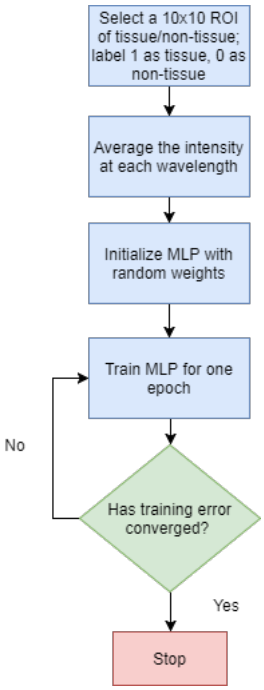

Fig. 2: Overview of the MLP training process

The goal of MLP training is to find the optimal weights that relate each input and node to one another. The MLP was trained via the back-propagation algorithm. First, the inputs are fed forward through the MLP (with the weights initially set to random values), with the output of each node in *l* layers modeled as:

$$o = f(\sum_{i=1}^{l} w_i x_i - \theta) \tag{2}$$

Where o is the output from the node, x is the input(s) to the node, w is the weight(s) to the input, and θ is a bias term [7]. The activation function, f, in this case is the sigmoid function. When the output propagates through the MLP, it is compared to the 'true' value of the output (i.e. the label of the input) with the following equation:

$$E(k) = \sum_{i=1}^{q} [t_i(k) - o_i(k)]^2 \tag{3}$$

The error, E, is defined as the square of the Euclidean norm of the k-th target output, where t is the target output, and o is the output of the i-th node [7]. Error must be minimized to give accurate results, therefore this error term serves as the objective function of the back-propagation algorithm. The back-propagation algorithm will iterate through epochs of training data until a convergence criteria is fulfilled. In this case, the goal is a training set error convergence of 1% (or until 20,000 epochs has been reached).

The full details of the back-propagation algorithm will not be discussed here (the algorithm is widely available in several texts [7]), but in general, an optimization problem is solved where E must be minimized by incrementally updating values of the weights (w) of each node.

3 Experimental Set-Up

To evaluate the MLP model, three sets of multispectral images were used as verification test data. Each image contained tissue and non tissue objects. These images were processed by the learned MLP model (i.e. learned weights and MLP architecture in Figure 1) using *MATLAB* software.

Each test image was fed into the MLP on a pixel by pixel basis. An example of a set of input images across the four wavelengths is presented in Figure 3.

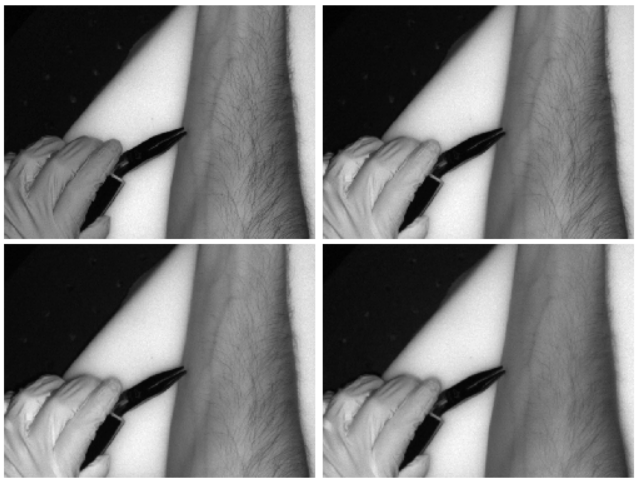

Fig. 3: An example of the MSI data/images that are inputs to the MLP. Top row, left to right: 740nm, 780nm. Bottom row, left to right: 850nm, 945nm

The resultant value given by the MLP is a decimal number between 0 and 1; for the purposes of these tests, any output greater than or equal to 0.5 was classified as 'tissue' and assigned a value of 1; conversely, non-tissue was assigned a value of 0.

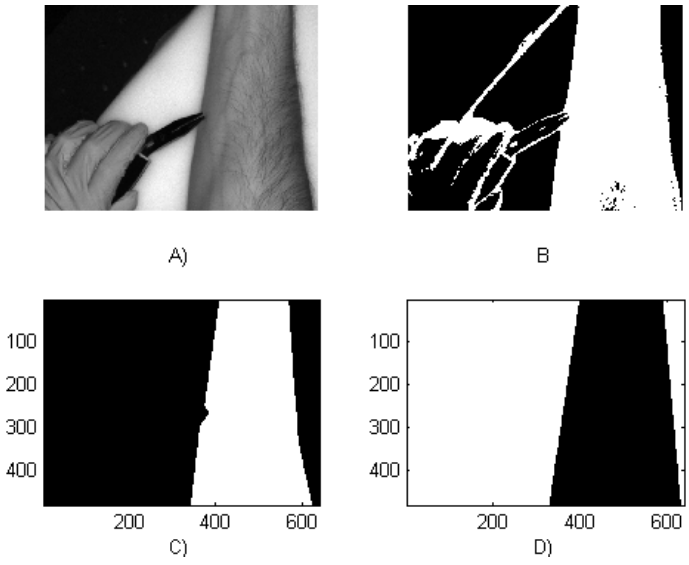

Fig. 4: A) A sample of the raw MSI data at 740nm, B) The processed MSI data by the MLP which yields a binary image; tissue in white, non tissue in black, C) Evaluation mask for known true tissue values, D) Evaluation mask for known true non-tissue values

After the images were processed, the accuracy, sensitivity, and specificity of the MLP must be determined to gauge its performance. For accomplishing this task, known tissue and non-tissue areas of the test images were manually marked on MATLAB software as shown in Figure 4C and Figure 4D. These areas were converted to 'masks' which were used to calculate the true positive, true negative, false positive, and false negative occurrences which are necessary for calculating accuracy, sensitivity, and specificity.

4 Results

Figure 5 shows, from a qualitative point of view, that edges and rapid depth changes have high occurrences of false positives for tissue. Also, areas that have greater noise due to prominent hair patches also show a visual occurrence of false negatives for tissue. The results from each test image are summarized in Table 1. The MLP shows excellent accuracy and sensitivity, however it has a comparatively low specificity.

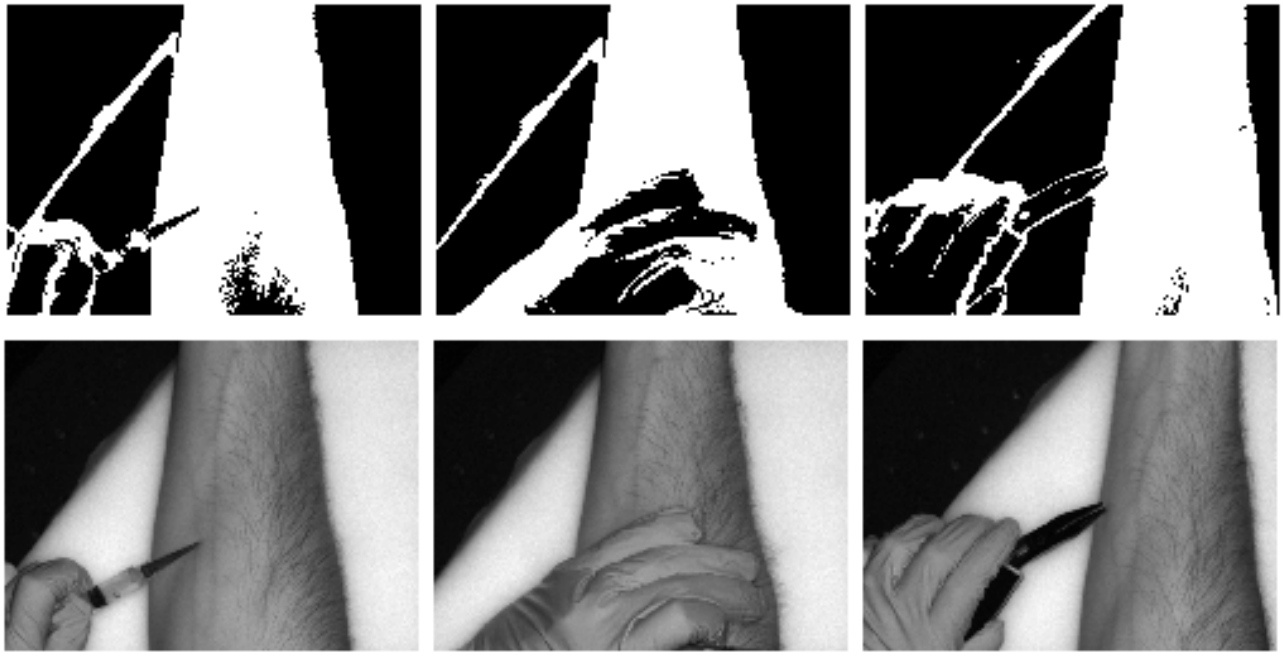

Fig. 5: Top row: the final output of the MLP for classifying tissue (white)/non-tissue (black) areas. Bottom row: The original images (740nm wavelength of each test set shown)

Table 1: Performance metrics of the MLP model against three test images

Test Image	Accuracy	Sensitivity	Specificity
1	0.9253	0.9484	0.9103
2	0.8900	1.000	0.8571
3	0.9241	0.9948	0.8856
Average	0.9131	0.9811	0.8843
S.D.	0.02	0.0284	0.0266

5 Discussion

The initial results are very encouraging, given that a high accuracy and sensitivity were found using a simple one-layer MLP. There is room for improvement as to handling areas of rapid depth transition such as edges and highly textured surfaces. Since this MLP only looks at using pixel-level spectra, there is no spatial context. Further research will explore methods that have spatial context to solve the tissue/non-tissue problem, such as Markov random fields and other graphical methods.

An attractive advantage of using a one-layer MLP is to have a fast and efficient classifier for real-time applications (relative to deep learning approaches). However, it is worthwhile to find the trade-off of using deep learning approaches when it comes to performance and computational time. This will also be an area of additional research.

Lastly, the work presented in this paper addresses tissue detection - to build upon the same concept, another area of future research could be to determine if this method is effective in classifying different types of tissues (i.e. different structures, cancers, etc).

6 Conclusion

This paper presented a novel MLP based on pixel-level spectra to determine regions of tissue/non-tissue in MSI datasets. We have demonstrated that this method is a viable solution for tissue detection/classification, and have shown average results of accuracy, sensitivity, and specificity of the algorithm at 91.3% (+/-0.2%), 98.1% (+/-0.3%), and 88.5% (+/- 0.3%) respectively.

Additional work will be carried out on incorporating spatial context into the MLP model as well as exploring other methods to improve the tissue/non-tissue classification performance.

Acknowledgments

We would like to thank NSERC, the NSERC Canada Research Chairs Program, as well as Christie Digital Systems for supporting this work.

References

[1] G. Lu and B. Fei, “Medical hyperspectral imaging: a review,” *Journal of Biomedical Optics*, vol. 19, p. 010901, jan 2014.

[2] J. M. Kainerstorfer, P. D. Smith, and A. H. Gandjbakhche, “Non-contact Wide-Field Multispectral Imaging for Tissue Characterization,” *IEEE JOURNAL OF SELECTED TOPICS IN QUANTUM ELECTRONICS*, vol. 18, no. 4, 2012.

[3] R. Jolivot, “Reconstruction of hyperspectral cutaneous data from an artificial neural network-based multispectral imaging system,” *Computerized Medical Imaging and Graphics*, vol. 35, mar 2011.

[4] M. Carrara, A. Bono, C. Bartoli, A. Colombo, M. Lualdi, D. Moglia, N. Santoro, E. Tolomio, S. Tomatis, G. Tragni, M. Santinami, and R. Marchesini, “Multispectral imaging and artificial neural network: mimicking the management decision of the clinician facing pigmented skin lesions,” *Physics in Medicine and Biology*, vol. 52, pp. 2599–2613, may 2007.

[5] S. Jacques, “Optical properties of biological tissues: a review,” *Phys. Med. Biol*, vol. 58, 2013.

[6] J. Cha, A. Shademan, H. N. D. Le, R. Decker, P. C. W. Kim, J. U. Kang, and A. Krieger, “Multispectral tissue characterization for intestinal anastomosis optimization,” *Journal of Biomedical Optics*, vol. 20, p. 106001, oct 2015.

[7] F. Karray and C. D. Silva, *Soft Computing and Tools of Intelligent Systems Design: Theory and Applications*. Pearson Addison Wesley, 2004.